

# Single-trial estimation of neuronal firing rates: From single-neuron spike trains to population activity

Martin Nawrot, Ad Aertsen, Stefan Rotter \*

*Neurobiology and Biophysics, Institute of Biology III, Albert-Ludwigs-University, Schänzlestraße 1, D-79104 Freiburg, Germany*

Received 15 July 1999; accepted 5 August 1999

## Abstract

We present a method to estimate the neuronal firing rate from single-trial spike trains. The method, based on convolution of the spike train with a fixed kernel function, is calibrated by means of simulated spike trains for a representative selection of realistic dynamic rate functions. We derive rules for the optimized use and performance of the kernel method, specifically with respect to an effective choice of the shape and width of the kernel functions. An application of our technique to the on-line, single-trial reconstruction of arm movement trajectories from multiple single-unit spike trains using dynamic population vectors illustrates a possible use of the proposed method. © 1999 Elsevier Science B.V. All rights reserved.

**Keywords:** Dynamic population vector; Dynamic spike responses; Kernel estimator; Neural coding; Single-trial rate estimation; Spike train analysis; Stochastic point process

## 1. Introduction

Most prevailing models of neural coding rely heavily on neuronal firing rates. It has been demonstrated in many physiological studies that the firing rate reveals relevant aspects of a neuron's involvement in information processing and computation. The availability of methods to measure firing rates from neuronal spike trains is therefore essential. The conventional strategy is to average the spike responses over repeated trials in the form of a peri-stimulus time histogram (PSTH; Gerstein and Kiang, 1960), and to interpret the outcome as an estimate of the time-varying rate function (Fig. 1). Using this technique, important insights into the neural mechanisms of sensory and motor processing have been gained.

There are, however, a number of problems with this approach: (1) Not all interesting experiments can be forced into a repeated-trial design; (2) averaging across trials requires stationarity across trials, which is not always guaranteed; (3) potentially relevant dynamic effects which are not strictly time-locked to the trigger

event do not survive trial-averaging. For these various reasons it is becoming increasingly important to eliminate the need for trial-averaging and to consider, instead, the alternative of estimating spike rates on the basis of single-trial responses. In addition, (4) the issue of trial-by-trial variability of neuronal responses is recently receiving increasing interest (Arieli et al., 1996; Azouz and Gray, 1999). Moreover, (5) certain multiple-electrode recording experiments (e.g. Chapin et al., 1999) create the need for a reliable on-line estimate of neuronal firing rates.

The firing rate is a fundamental concept for the description of a spiking neuron (and a point process in general; Cox and Isham, 1980). The underlying firing rate  $\rho(t)$ , also termed intensity function, is a non-negative deterministic function of time, such that the integral

$$\int_{t_a}^{t_b} \rho(t) dt \quad (1)$$

represents the expected number of spikes encountered in an observation of the neuron during the observation interval  $[t_a, t_b]$ .

In the context of the current paper, the underlying rate function is assumed to be invariant across trials. In reality, this rate function may change as a result of

\* Corresponding author. Tel.: +49-761-2032862; fax: +49-761-2032860.

E-mail address: rotter@biologie.uni-freiburg.de (S. Rotter)

circumstances beyond the control of the experimenter. However, even if the rate function is the same over trials, individual spike trains in repeated observations may vary considerably, as a result of random fluctuations. The underlying rate is nevertheless reflected by the instantaneous density of spikes.

The rate function underlying the spiking of a real neuron, however, cannot be observed directly, it must be reconstructed from the recorded spike trains. Unfortunately, the theory of stochastic point processes does not currently provide a substantial apparatus for the direct inference of underlying dynamics from experimental data. Here, we describe a method to estimate the neuronal firing rate from single-trial spike trains by convolution with a fixed kernel function. The method is calibrated on the basis of simulated spike trains for a selected set of typical dynamic underlying rate functions. From this we derive rules for the optimized use and performance of the kernel method. Finally, we present an application of our technique to the on-line, single-trial reconstruction of arm movement trajectories from multiple single-unit spike trains using dynamic population vectors. Preliminary results have been presented in abstract form (Nawrot et al., 1997, 1999).

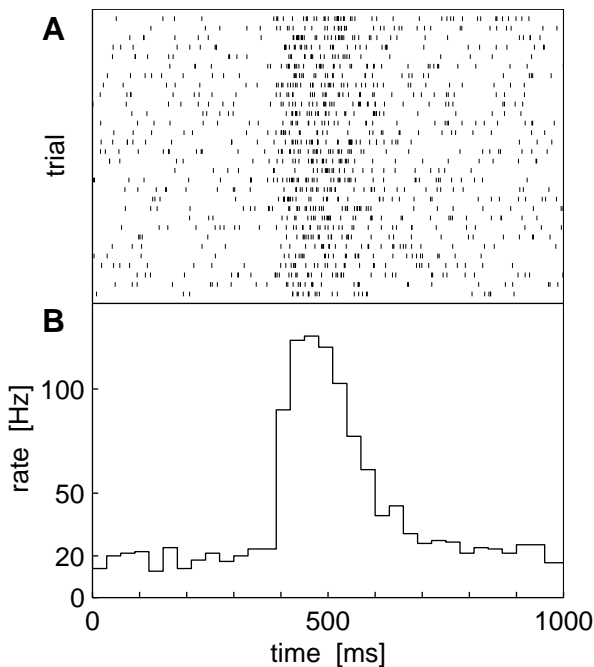


Fig. 1. Rate estimation by means of trial-averaging: the peri-stimulus time histogram (PSTH). (A) Raster display of spike events for 30 trial repetitions. (B) PSTH of average spike response, constructed from all 30 trials using a bin size of 30 ms.

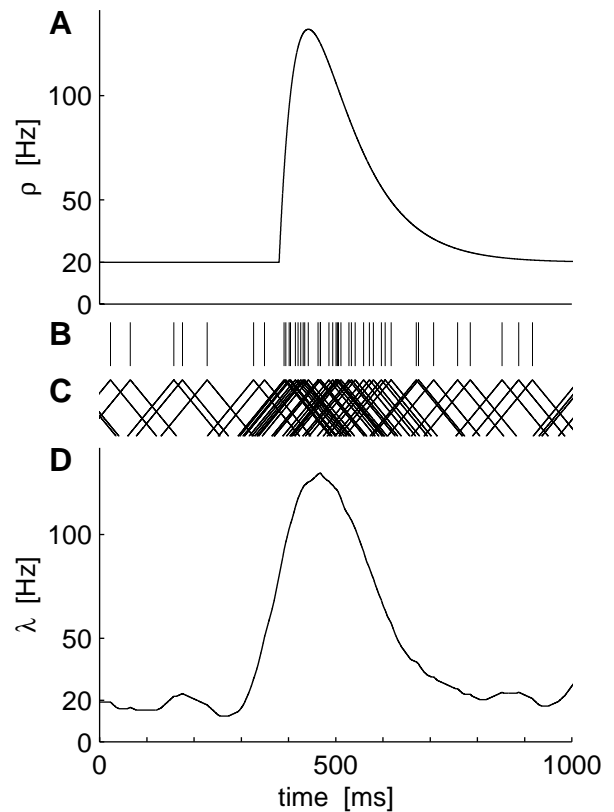


Fig. 2. Concept of single-trial rate estimation by means of the kernel approach. The ‘true’ underlying rate function  $\rho(t)$  shown in (A) is estimated from one single-trial spike train (B) by taking the sum over kernel functions  $K(t-t_i)$ , centered at spike occurrence times  $t_i$  (C), yielding the empirical rate function  $\lambda(t)$  shown in (D). In this particular example, a triangular kernel with a standard width of  $\sigma = 40$  ms was used.

## 2. Methods

### 2.1. Estimation

Consider a single spike train, comprised of a finite number of discrete spike events at times  $t_1, \dots, t_n$ . We define the estimation of the time-varying rate function as

$$\lambda(t) := \sum_{i=1}^n K(t-t_i) \quad (2)$$

where  $K(t)$  is called kernel function. Thus, the desired underlying ‘true’ rate function is estimated from a single-trial spike train by taking the sum over kernel functions  $K(t-t_i)$ , centered at spike occurrence times  $t_i$  (Fig. 2).

We require  $K(t)$  to be non-negative to avoid negative rates. Moreover, the kernel should be normalized such that each spike contributes with unit area to the rate function. This guarantees that the integral of  $\lambda(t)$  is equal to the total number of spikes  $n$  recorded during

Table 1  
Tested kernel functions<sup>a</sup>

Kernel	$K(t, \sigma)$	Support
Boxcar	$\frac{1}{2\sqrt{3}\sigma}$	$[-\sqrt{3}\sigma, \sqrt{3}\sigma]$
Triangle	$\frac{1}{6\sigma^2}(\sqrt{6}\sigma -  t )$	$[-\sqrt{6}\sigma, \sqrt{6}\sigma]$
Epanechnikov	$\frac{3}{4\sqrt{5}\sigma} \left(1 - \frac{t^2}{5\sigma^2}\right)$	$[-\sqrt{5}\sigma, \sqrt{5}\sigma]$
Gauss	$\frac{1}{\sqrt{2\pi}\sigma} \exp\left(-\frac{t^2}{2\sigma^2}\right)$	$[-\infty, +\infty]$

<sup>a</sup> Outside the support, the kernels are defined to be zero. All kernel functions are normalized to unit area and have standard width  $\sigma$ .

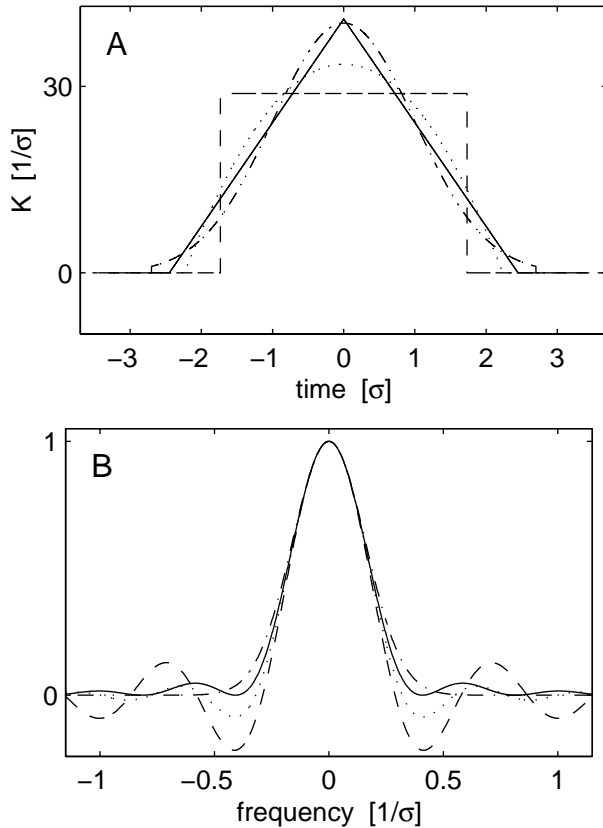


Fig. 3. Tested kernel functions (—Triangle, -- Boxcar, ··· Gauss, ···· Epanechnikov). All kernels have unit area and are parametrized according to their standard width  $\sigma$  (cf. Table 1). (A) Time course and (B) Fourier transforms of kernel functions.

the observation interval. Finally, we require the first moment of  $K(t)$  to be zero to preserve the center of mass of the spike train. Taken together, this leads to the following constraints on the kernel function:

$$K(t) \geq 0, \quad (3a)$$

$$\int_{-\infty}^{\infty} K(t) dt = 1, \quad (3b)$$

$$\int_{-\infty}^{\infty} t K(t) dt = 0. \quad (3c)$$

The properties of the estimation depend on the properties of the specific kernel function chosen. Two aspects are important: the shape of the kernel function and its width. The kernel shape determines the visual appearance of the estimated rate function. The standard width of the kernel

$$\sigma = \sqrt{\int_{-\infty}^{\infty} t^2 K(t) dt} \quad (4)$$

specifies the temporal resolution of the rate estimation. Hence,  $\sigma$  can be viewed as a smoothing parameter. Table 1 lists the four kernel functions of different shapes that we tested, parametrized by their standard width. Fig. 3 shows the time course and Fourier transform of these four types of kernels.

Kernel estimators are widely used and treated theoretically in the context of density estimation (Parzen, 1962; Silverman, 1986; Scott, 1992; Bowman, 1997). The method has also been proposed for estimating neuronal firing rates by various authors (Sanderson, 1980; Richmond et al., 1987, 1990; Paulin, 1992; Nawrot et al., 1997; Szűcs, 1998).

## 2.2. Calibration

To test the kernel estimator method we employ a calibration procedure on the basis of simulated spike trains, generated according to pre-set underlying rate functions with a variety of parametrized dynamics. The calibration involves three steps. First, we specify the stochastic point process used for generating spike data. Second, we choose a representative class of underlying rate functions that will be used for the simulations. Third, we define a quality measure with which we can assess the performance of the rate estimation.

### 2.2.1. The Poisson process

The underlying rate function is only partially specifying the point process, it represents its ‘deterministic’ aspects. The actual stochastic properties of spike generation are reflected by the probability distribution of the spike counts for each observation interval.

In the context of neuronal modeling, the most frequently used type of stochastic point process is the Poisson process. In fact, it is the most elementary type of stochastic point process (Cox and Isham, 1980). The points occur independently of each other, governed only by the rate function. As a consequence, the spike counts have a Poisson distribution with both mean and variance given by expression (1). The simplicity of the Poisson model supports the generation of computer-simulated spike trains, while being not too remote from real spike trains recorded from physiological neurons.

Table 2

Simulation parameters for the dynamic rate function  $\rho(t)$ : constant background rate  $b$ , response strength  $A$  and response width  $w$ <sup>a</sup>

$b$ [Hz]	1	2	5	10	20	30	40	50	–
$A$ [spikes]	0	5	10	20	30	40	50	80	100
$w$ [ms]	10	20	30	40	50	80	100	150	200

<sup>a</sup> The parameter space tested is spanned by a selection of triple combinations ( $b$ ,  $A$ ,  $w$ ) taken from this set.

### 2.2.2. A family of rate functions

Next, we have to define a class of realistic dynamic rate functions  $\rho(t)$  that resemble typical PSTHs from in vivo single-unit spike recordings. For this purpose we chose a parametric family of phasic response profiles, superimposed on a stationary background of adjustable strength. All parameters were subject to systematic variation. The phasic response was selected to be proportional to a beta-function

$$\beta_{\tau_1, \tau_2}(t) := \begin{cases} \frac{1}{\tau_1 - \tau_2} \left( e^{-\frac{t}{\tau_1}} - e^{-\frac{t}{\tau_2}} \right) & \text{for } t > 0 \\ 0 & \text{for } t < 0 \end{cases} \quad (5)$$

where  $\tau_1 > \tau_2 > 0$  are the falling and rising time constants, respectively. Here,  $\beta_{\tau_1, \tau_2}(t)$  is normalized to unit area, and its standard width is given by

$$w = \sqrt{\tau_1^2 + \tau_2^2}. \quad (6)$$

We finally define the following class of intensity functions

$$\rho_{b,A,w}(t) := b + A \beta_{\tau_1, \tau_2}(t - t_0), \quad \text{with } \tau_1 = 2\tau_2 \quad (7)$$

where  $t_0$  denotes the time of response onset. Thus, we have three parameters that capture the essential properties of the underlying rate function. The constant background rate  $b$  accounts for spontaneous activity. The response strength  $A$  is the integral over the phasic excitatory response; it measures the expected number of spikes exceeding spontaneous activity. The temporal extent of the response is characterized by its standard width  $w$ .

To test the performance of the rate estimation, we generated sets of repeated trials of artificial spike train data for a variety of choices for the parameters ( $b$ ,  $A$ ,  $w$ ) according to Table 2. We made sure that the scanned parameter range covers dynamic rate functions as they are typically observed in physiological recordings from a variety of brain areas, including critical cases with weak responses, possibly in the presence of high background rates. Time-inverted versions of these rate functions are implicitly covered by our analysis, because all tested kernels are symmetrical. An example for a rate function with parameters  $b = 20$  Hz,  $A = 20$

spikes and  $w = 100$  ms is shown in Fig. 2A. Thirty Poisson realizations using this underlying rate function are shown in Fig. 1A.

### 2.2.3. Measure of performance

To evaluate the performance of the rate estimator (Eq. 2) we use the integrated square error (Silverman, 1986; Scott, 1992)

$$\text{ISE} := \int_0^T (\lambda(t) - \rho(t))^2 dt \quad (8)$$

as a global measure of the discrepancy of the estimated rate function  $\lambda(t)$  from the underlying rate function  $\rho(t)$ . The integral was computed for a fixed observation interval, which we chose to begin 100 ms before response onset and to end 400 ms after it. The better the agreement between the underlying rate function  $\rho(t)$  and its estimate  $\lambda(t)$ , the lower the value of ISE. An example for visual comparison of underlying and estimated rate functions is shown in Fig. 2A and D, respectively.

For each intensity function  $\rho_{b,A,w}(t)$ , we simulated an ensemble of  $N = 100$  trials. From each spike train we then estimated a single-trial rate function and calculated the ISE with respect to  $\rho_{b,A,w}(t)$ . As a measure for the performance of the rate estimation method for ensembles of trials we used the mean integrated square error

$$\text{MISE}_N := \langle \text{ISE} \rangle_N = \frac{1}{N} \sum_{j=1}^N \int_0^T (\lambda_j(t) - \rho(t))^2 dt \quad (9)$$

as the mean ISE for  $N$  single-trial estimations  $\lambda_j(t)$  of the same underlying rate function  $\rho(t)$ .

## 3. Results

The results of our calibration procedure, expressed in terms of the mean integrated square error MISE, show how the performance of the rate estimation depends on shape and width of the kernel function. Based on a systematic variation of the parameters ( $b$ ,  $A$ ,  $w$ ), we derived rules for the construction of optimized kernels when applying the method to experimental data.

### 3.1. Influence of kernel shape

In the case of constant spike rates, i.e. in the absence of a phasic response, the four kernel shapes perform virtually identically, independent of the rate level. As can be seen for a typical example in Fig. 4A, the four kernel shapes can hardly be distinguished on the basis of their MISE values. The standard deviation of ISEs, calculated from an ensemble of single-trial estimates with a Triangle kernel, is larger than the differences between mean values for different kernel shapes.

In the case of time-varying rates ( $A > 0$ ) we obtained the same result. Different kernels perform equally well over a broad range of kernel widths. As shown in the example of Fig. 4B, the main features of the graphs are present for all four kernel shapes. In particular, for optimal choice of  $\sigma$ , the difference in performance for different kernel shapes is negligible. This finding is in good agreement with theoretical results given in Silverman (1986) and Scott (1992).

From these results we can draw the conclusion that the choice of a specific kernel shape is not critical for the estimation error. Thus, the choice of the kernel shape can be based on other considerations, in particular visual appearance (e.g. smoothness) of the estimated rate. The latter is determined by the filter properties of the kernel function, which can be inferred from its frequency spectrum (Fig. 3B).

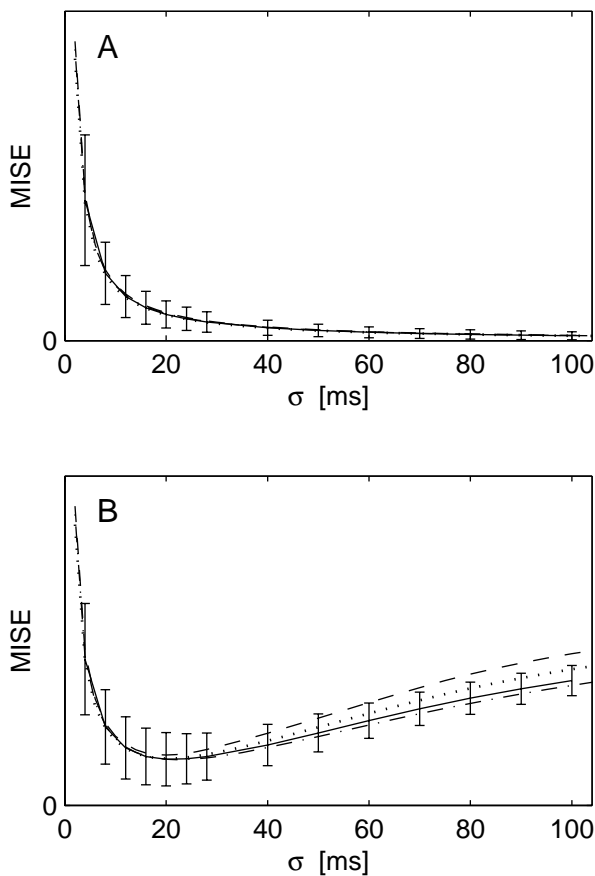


Fig. 4. Performance of rate estimation for different kernel shapes, depending on the kernel width  $\sigma$ . Line styles as in Fig. 3. Error bars denote the standard deviation of the integrated square error from 100 single-trial estimations with a Triangle kernel. (A) MISE as a function of  $\sigma$  for the estimation of a constant rate with  $b = 10$  Hz. (B) MISE as a function of  $\sigma$  in the case of a time-varying rate function with simulation parameters  $b = 10$  Hz,  $A = 20$ ,  $w = 50$  ms. The estimate is optimal for  $\sigma \approx 20$  ms, independent of the kernel shape. For both constant and transient rate functions, the choice of the kernel shape has almost no influence on the performance of the rate estimation.

The results shown in Fig. 4 also indicate that the standard width is a good choice for parametrizing the temporal resolution of  $K(t)$  with respect to the comparability of kernel shapes.

Computational costs scale with the extent of the support, i.e. the domain over which the kernel function assumes non-zero values. This parameter is comparable for all kernels, with the exception of the Gaussian kernel. This latter kernel, predominant in earlier publications on this subject, must be constrained to a reasonable finite support (cf. Fig. 3A) to be competitive with respect to computational costs. All results presented in subsequent sections are based on estimations using a Triangle kernel.

### 3.2. Influence of kernel width

#### 3.2.1. Constant rates

Fig. 5 summarizes the performance of the kernel estimator for stationary spike rates. Specifically, we analyzed the dependence of the estimation error MISE on spike rate  $b$  and kernel width  $\sigma$ . Fig. 5A generalizes the result obtained in Fig. 4A for different firing rates  $b$ . In each case, we observe a monotonic decrease of MISE with increasing kernel width  $\sigma$ . As was to be expected for a constant rate, a better estimate of the rate is obtained for a wider kernel.

When comparing the performance of the kernel estimator for different values of the spike rate, we observe an increase of MISE and, hence, a decrease of performance with rate. This is a straightforward result of the statistical properties of the Poisson process: the variance of the spike count increases with its rate. This, in fact, suggests to normalize the MISE by dividing it by the variance of the total spike count, which is proportional to the rate  $b$  in the case of a Poisson process. Indeed, Fig. 5B shows that the variance-normalized MISE is independent of the spike rate, apart from statistical fluctuations.

#### 3.2.2. Time-varying rates: variation of response duration

We now turn to the performance of the kernel estimator for time-varying rate functions. In our simulations, this is accomplished by having a phasic response component, characterized by its response strength  $A$  and duration  $w$ , superimposed on a constant background  $b$ .

We first consider the dependence of the estimator performance on the kernel width  $\sigma$  under variation of the response duration  $w$ . The response strength  $A$  and background level  $b$  are kept fixed. The results are summarized in Fig. 6. Observe that for each choice of response duration there exists a unique optimal choice of kernel width  $\sigma$ . For instance, in the case of  $w = 50$  ms, best performance is achieved for  $\approx 20$  ms,

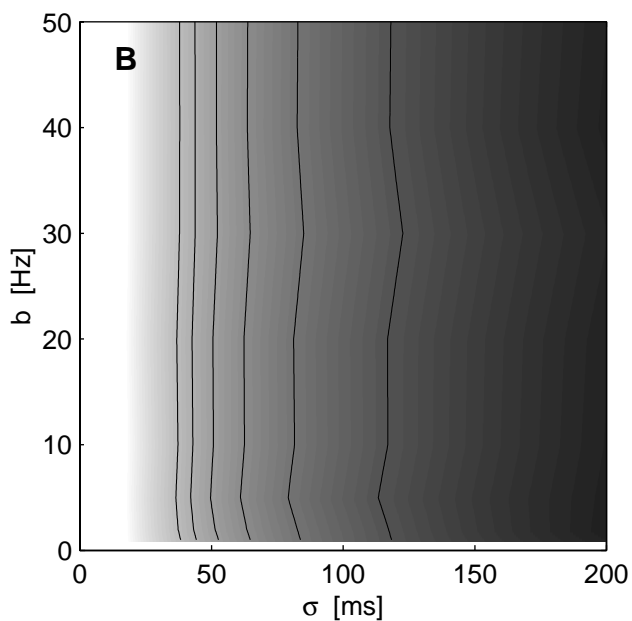
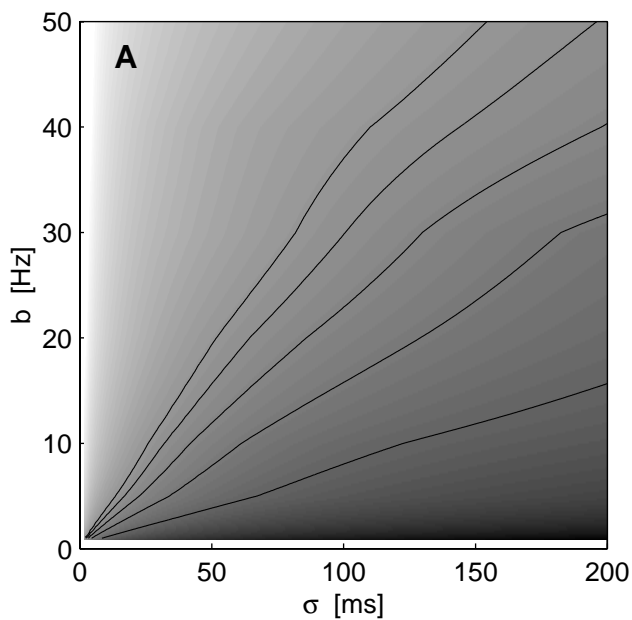


Fig. 5. Performance of rate estimation for constant rates  $b$ , depending on the kernel width. (A) Absolute error (MISE), (B) variance-normalized error (MISE/ $b$ ). Gray code using arbitrary units, darker regions represent better performance (low MISE resp. MISE/ $b$ ), lighter regions represent worse performance (high MISE resp. MISE/ $b$ ). Contour lines are drawn for equidistant levels of MISE and MISE/ $b$ , respectively.

coinciding with the shorter of the two time constants governing the rate dynamics (Eq. 5). For the parameter range shown here, the optimal choice of kernel width increases approximately linearly with the response duration, as indicated by the dashed line in Fig. 6.

This result confirms our expectation that the fastest time constants of the underlying rate dynamics deter-

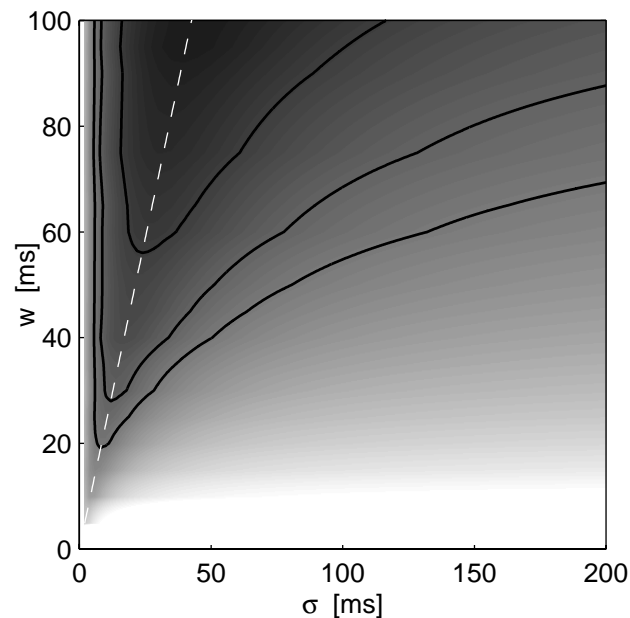


Fig. 6. Dependence of rate estimation performance on kernel width, under variation of the duration  $w$  of the phasic response. Background rate  $b = 10$  Hz and response strength  $A = 20$  spikes are fixed. Gray code as in Fig. 5; contour lines are drawn for equidistant MISE levels. Dashed line fitted to minimum values of MISE.

mine the optimal time resolution to be chosen in the analysis. Conversely, the time resolution chosen in the analysis poses a lower bound for the time constants of the dynamics that can be reliably reconstructed.

### 3.2.3. Time-varying rates: variation of response strength and background rate

Next, we consider the dependence of the estimator performance on the kernel width  $\sigma$  under variation of the response strength  $A$ . Now, the response duration  $w$  and background level  $b$  are kept fixed. The results are shown in Fig. 7A.

Observe that for large enough response strength  $A$ , there exists a clear minimum of the MISE, and an associated optimal choice of  $\sigma$  close to the shorter time constant of the response transient. For increasing values of  $A$ , this optimum slowly shifts towards smaller values of  $\sigma$  (cf. dashed line in Fig. 7A). Hence, for weak phasic responses, the temporal resolution of the rate estimation is reduced. As in Fig. 5, the gradual decrease of MISE values for smaller  $A$  reflect the decrease in variance of the corresponding spike counts.

Analogous conclusions can be drawn from the results of variation of the background rate  $b$  (Fig. 7B). A similar behavior of the optimal kernel width  $\sigma$  as in Fig. 7A is obtained, provided we replace a decrease of  $A$  by an increase of  $b$ . This underlines the dual roles of

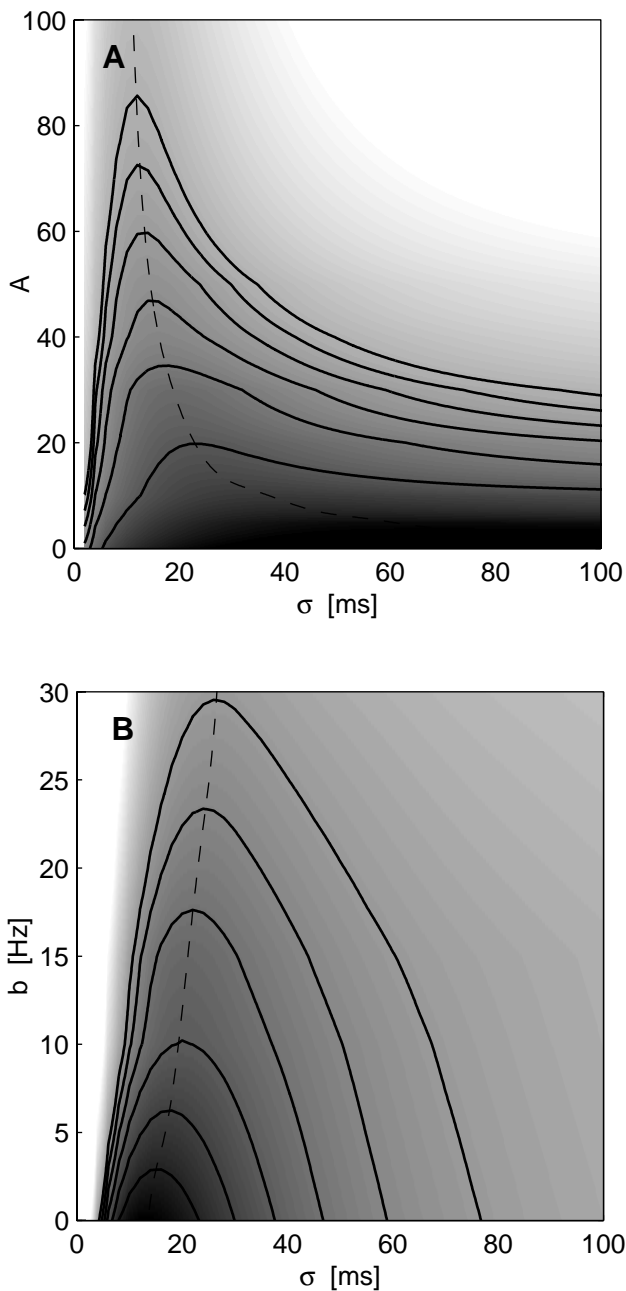


Fig. 7. Dependence of rate estimation performance on kernel width, under variation of (A) the strength  $A$  of phasic response and (B) the background rate  $b$ . In (A) the background rate  $b = 20$  Hz and response duration  $w = 50$  ms. In (B) the response strength  $A = 5$  and response width  $w = 20$  ms. Gray code as in Fig. 5; contour lines are drawn for equidistant MISE levels. Dashed lines fitted to minimum values of MISE.

these two parameters of the response. By contrast, both an increase in  $A$  and an increase in  $b$  lead to an increase in total spike count. As a consequence, in both cases the variance is increased, implying larger values for the MISE, as is reflected by the similarity of gray gradients in both Fig. 7A and B.

### 3.2.4. Rules for optimized use and performance of the kernel method

Given a measured spike train, we will now outline two possible and complementary strategies for finding an optimized kernel to be employed for single-trial rate estimation.

The first strategy is based on the availability of sufficient pre-knowledge about the underlying rate function. Calibration plots as discussed in the previous sections can then be used to determine a kernel which promises (near-)optimal rate estimators. The results from our numerical analyses have been cast into a set of rules to guide the user in the search for the optimal kernel (see Table 3). Starting from educated guesses of the temporal width  $w$ , the strength  $A$  of the response, and the intensity  $b$  of the background rate, one can read out the width  $\sigma$  of the best-performing kernel from the corresponding calibration plots as in our Figs. 5–7. Iterative improvement by repeated application of this procedure might recommend itself.

The second strategy, in contrast, does not rely so much on pre-information and user interaction. The non-monotonic dependence of the MISE on kernel width, especially at larger values of the response strength  $A$  and low values of the background rate  $b$ , suggests an alternative approach to determine the unknown rate dynamics underlying an experimentally-recorded spike train. By systematically reducing the kernel width  $\sigma$  and evaluating the ISE for pairs of successive rate estimates associated with these kernels, one typically encounters a more or less clear minimum in this measure of difference, located at some critical value of the kernel width  $\sigma$ . We applied this unsupervised search procedure to a number of single-trial spike trains for a representative selection of underlying rate functions. The results are shown in Fig. 8. Observe that in most cases considered, this procedure indeed yields a clear minimum, provided the response is not too weak or too wide. In each case, we also show the width of the kernel which was found to be optimal according to our previously stated criteria (dotted lines in Fig. 8). We found very good agreement between these two numbers, in all cases examined. Hence, the location of the minimum in our iterative procedure provides a useful estimate of the optimized kernel width, even in the absence of prior information on the underlying rate dynamics.

We applied both strategies for determining an optimized kernel width to real spike trains recorded from single neurons of the monkey motor cortex. For such data, obviously, no reference to a known underlying rate function is possible. Nevertheless, in all cases considered the unsupervised search yielded an unequivocal prescription of an optimized kernel width  $\sigma$ . Depending on the characteristics of the particular data set, this

optimized kernel width was in the range of a few tens of milliseconds. Again, it was possible to confirm this estimate by an application of the first method, starting

out from rough estimates of the response parameters obtained by visual inspection of the raw spike trains. The possibility to cross-validate the results, an applica-

Table 3  
Rules for optimized use and performance of the kernel method<sup>a</sup>

Rule	Figures
Stationary rates	
1 The wider the kernel the better	4A, 5A, B
Transient rates	
2 Kernel shape not important	4A, B
3 Kernel width must be tuned for optimal performance, depending on response strength, response duration, and background rate	4B, 6, 7A, B
4 Unique optimal kernel width exists and is proportional to (fastest) time constant decreases with increasing response strength increases with increasing background rate	6 7A 7B

<sup>a</sup> These results are based on an evaluation of the MISE for numerical simulations of a representative and physiologically plausible selection of dynamic rate functions.

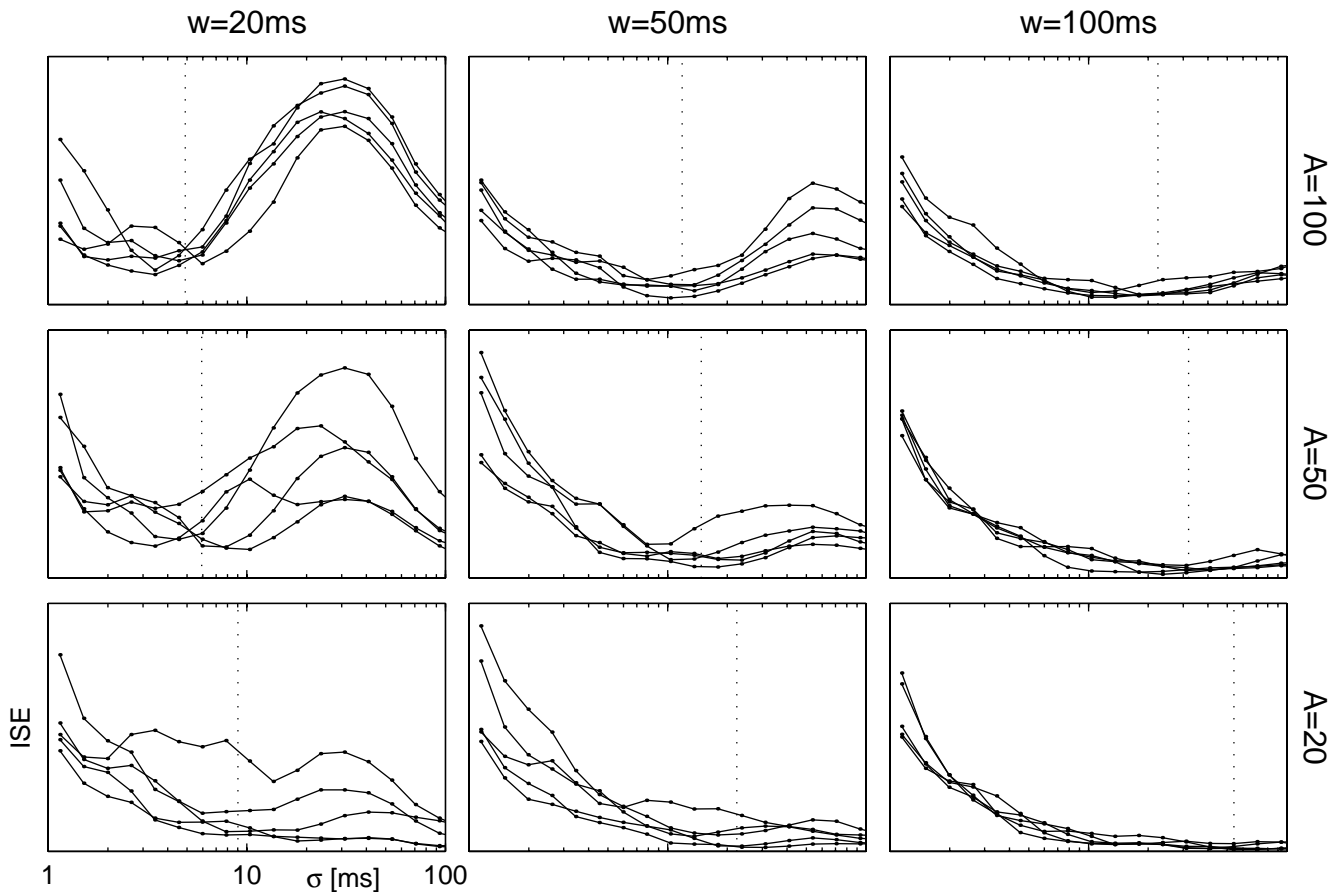


Fig. 8. Unsupervised search to identify optimized kernel width for single trial spike trains. Each curve shows the ISE between successive rate estimates, determined by progressively decreasing the kernel width  $\sigma$  by equidistant steps on a logarithmic scale. Each frame shows the results for five individual trials of spike data for a particular choice of response strength  $A$ , response duration  $w$ , and background rate  $b$ . Different frames correspond to representative selections of response strength  $A$  and response duration  $w$ ; the background rate  $b = 20$  Hz was fixed in all cases. Observe that in most cases the ISE curves show a more or less clear minimum, provided the response is not too weak or too wide. For comparison with previous results, obtained from direct comparison of the reconstructed rates with the known underlying rate function, the dotted lines indicate the kernel width for which the estimator showed best performance in terms of MISE (dashed line in Fig. 7 A). In each row of frames all ordinates are scaled identically.

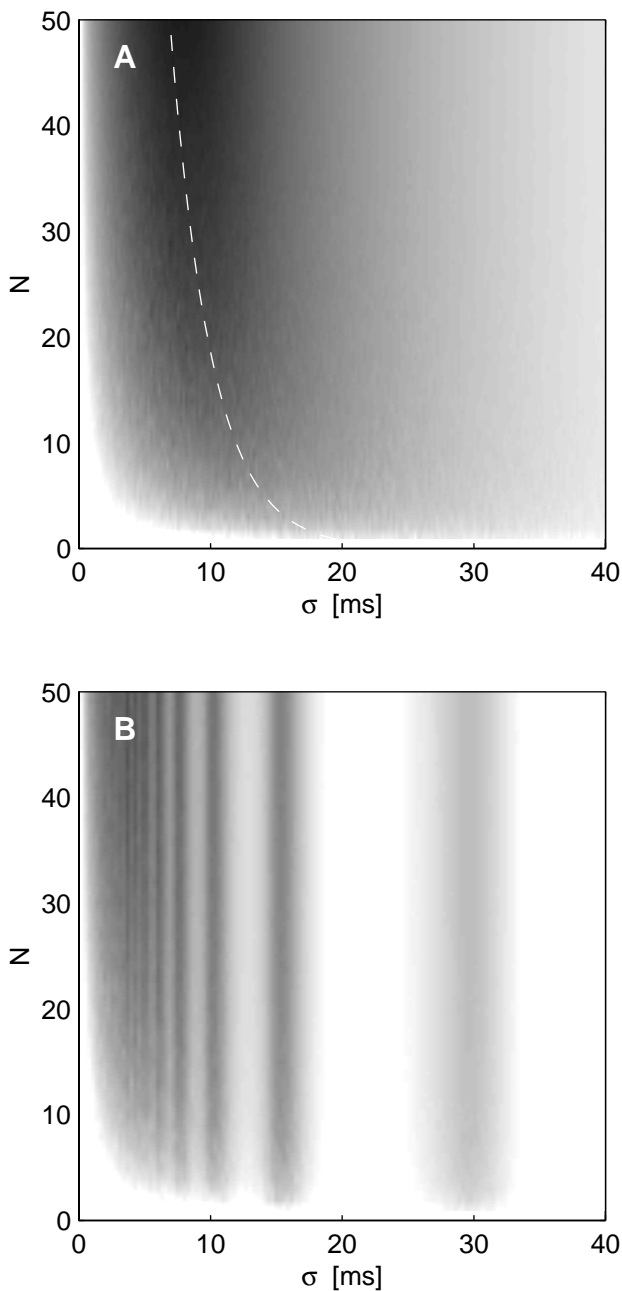


Fig. 9. Performance of trial-averaged kernel estimation in comparison with the PSTH. Shown is the MISE of reconstructed rates for randomly drawn ensembles of  $N$  trials for (A) trial-averaged kernel estimates using a triangular kernel of width  $\sigma$  and (B) conventional PSTH estimates using bins of width  $2\sqrt{3}\sigma$  matched to the standard width  $\sigma$  of the Boxcar kernel. Example for fixed simulation parameters  $b = 20$  Hz,  $A = 20$ ,  $w = 50$  ms. Gray scales for MISE values are identical in both plots. Dashed line fitted to minimum values of MISE.

tion of a dual strategy as outlined above is, therefore, our strong recommendation.

### 3.2.5. Time-varying rates: trial-averaging

So far we have evaluated the performance of our rate

estimator for single-trial estimates. Now we will consider the question how good the kernel estimator performs as a trial-averaging technique in comparison with the classical method of constructing a PSTH. To this end, we perform rate estimation for each single-trial separately and average the resulting rate estimates across a number of trials before evaluating the ISE.

Exemplary results are shown in Fig. 9. In the case of kernel estimation (Fig. 9A) there exists a unique optimal kernel width  $\sigma$  for any number of trials  $N$ . As could be expected, the temporal width of the kernel may be chosen smaller, the more trials are available. Thus, the temporal resolution that can be attained by the rate estimate improves with the number of trials  $N$  (cf. dashed line in Fig. 9A). The integrated square error decreases approximately with the square root of  $N$ .

In comparison, the results of PSTH performance (Fig. 9B) show that there is no optimal bin width for constructing the histogram. The vertical stripes in this Figure are a Moiré-type pattern, reflecting the misalignment of the discrete binning grid with the response onset  $t_0$  (cf. Section 2.2.2). Only if  $t_0$  lies exactly on the grid, the region around the response onset is faithfully captured by the PSTH.

In general, on the basis of a fixed number of trials, the kernel estimator performs decisively better than the PSTH. In practical terms, this implies that kernel estimation needs considerably fewer trials than the histogram approach to achieve an equally good rate reconstruction.

Note that in our simulations we did not introduce any trial-specific latency variations for the response onset  $t_0$ . Such latencies are, however, often present in experimental data where repeated trials are not strictly time-locked to the response-inducing event (typically a stimulus) (Sanderson, 1980; Richmond et al., 1990; Nawrot et al., 1999). In the presence of such latency variations, the binning artifact will be diminished. Evidently, in this case, straightforward trial-averaging is bound to decrease the peak performance of both the PSTH and the kernel estimator. More sophisticated techniques, based on a realignment of trials, may then be invoked to obtain a faithful portrait of the dynamic rate functions (Sanderson, 1980; Nawrot et al., 1999).

### 3.3. Application to single-trial population vector

In the previous sections we were mainly concerned with ascertaining ourselves that the kernel estimator yields a reliable estimate of the underlying rate functions. Now, we will explore an application of the method that specifically addresses two other important aspects: the possibility of on-line estimation, combined with having access to the simultaneous activities of multiple-single neurons. This application, in fact, resembles earlier approaches to reconstruct the sensory

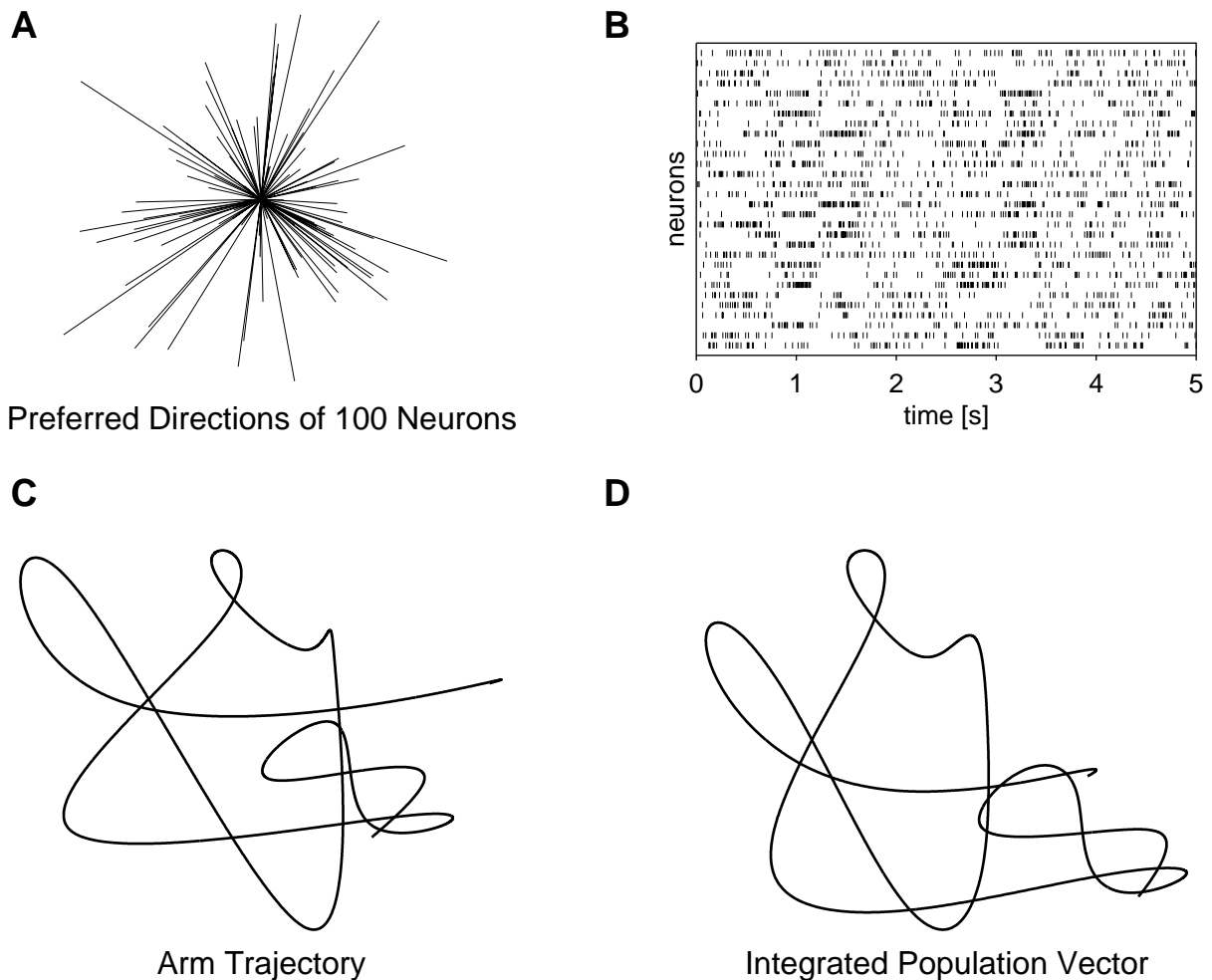


Fig. 10. Representation of a fast 2D arm movement by simultaneous spike trains of a recorded population of 100 neurons. (A) Preferred directions of all neurons contributing to the population vector, length of the vectors indicate velocity tuning. (B) Spike trains of a representative sample of 30 neurons. An average firing rate between 10 and 25 Hz and Poisson statistics were used in the simulations. (C) Simulated hand trajectory, giving rise to the neuronal spike trains is shown. Observe how the frequent turns during the initial phase of the movement are reflected in dynamic changes in the firing rates. (D) Reconstructed movement trajectory, obtained by integration of the population vector. The firing rates were computed from the spike trains without averaging by using the kernel method (Triangle,  $\sigma = 75$  ms).

interpretation of multi-neuron spike trains (Johannesma, 1981; Gielen et al., 1988; Hesselmann and Johannesma, 1989).

The on-line computation of time-dependent neuronal population vectors (Georgopoulos et al., 1982; Schwartz, 1994) from simultaneously recorded spike trains can be achieved by a straightforward application of the kernel method. Trial-averaging is not necessary, if (1) the neuronal population is large enough, (2) the preferred directions of the individual neurons are uniformly distributed, and (3) the parameters of the kernel are carefully chosen. An application to real-time control of reaching movements of a robot arm on the basis of simultaneously recorded motor cortex neurons in extension to Chapin et al. (1999) thereby becomes feasible.

We tested the performance of this approach on the basis of computer simulated spike trains, assuming a

population of motor cortex neurons with realistic directional and velocity tuning (Moran and Schwartz, 1999). If the directional tuning of a neuron follows a cosine law, its firing rate  $f(t)$  depends on the current velocity vector  $\vec{v}(t)$  of the movement according to

$$f(t) = f_0 + \vec{p} \cdot \vec{v}(t) \quad (10)$$

where  $f_0$  is the background firing rate and  $\vec{p}$  is the preferred movement direction of the neuron. The modulation of the firing rate  $\vec{p} \cdot \vec{v}(t)$  is proportional to the velocity of the movement, the length of the preferred vector  $\vec{p}$  encodes the gain for velocity. For a randomly sampled population of motor neurons, the preferred vectors  $\vec{p}$  are broadly distributed, more or less evenly covering all possible directions.

We used the kernel method to reconstruct the time course of the firing rate for each neuron of the population individually. On the basis of these rates, and

assuming that the preferred directions and velocity gains of all neurons are known, the time-dependent population vector can be constructed in the usual way. Temporal integration of this population vector then yields a trajectory in space, which matches the trajectory of the original arm movement in very good approximation (Fig. 10). A quantitative evaluation of this procedure for real multi-neuron spike data is currently in progress. As was to be expected, the reconstructed representation improves with the size of the population. We found that, for the relatively fast type of movement shown, a population of only 50–100 neurons suffices to achieve a surprisingly high quality of movement representation. Such numbers are rapidly becoming feasible using state-of-the-art multi-electrode recording techniques (Nicollelis, 1998).

#### 4. Discussion

We described a method to estimate the neuronal firing rate from single-trial spike train data. The method, basically a convolution of the spike train with a fixed kernel function, was calibrated on the basis of simulated spike trains. Our findings demonstrate that estimation of neuronal firing rates from single-trial spike trains is feasible for a representative selection of physiologically realistic dynamic spike responses, including difficult cases with weak responses against a relatively strong background. On the basis of these results, we derived rules for the optimized use and performance of the kernel method, specifically with respect to an effective choice of the shape and width of the kernel functions.

To better localize sharp edges and other fast transients of the underlying rate function (e.g. to extract the response latency or the slope at response onset), the use of asymmetric, causal or anti-causal, kernel shapes suggests itself. However, judged by the ISE measure, their use did not lead to improved rate estimates for the family of dynamic rate functions examined. To selectively assess the performance of rate estimators with respect to such local features of the underlying rate function, different (non-integral) measures can be constructed. The potential of such extended methods is currently being explored. Further experiments in our laboratory using extensions of the basic method (including adaptive kernels, Savitzky–Golay filters (Diesmann et al., 1996) and more general non-linear rate estimators (Nawrot et al., 1997)) yielded promising results. So far, however, they were not found to be widely applicable, primarily because the additional parameters make them less manageable and, accordingly, they still require too much user intervention.

We are currently testing the applicability of single-trial rate estimates also in the context of other types of spike train analyses. A particularly important application in this respect concerns their use as control measurements

against which to test multiple single-unit spike data for the presence of dynamic spike synchronization phenomena (Gerstein and Aertsen, 1985; Aertsen et al., 1987, 1989; Riehle et al., 1997; Grün et al., 1999).

The approach of single-trial estimation of neuronal firing rates opens the way to address a number of questions that were previously impossible to be treated with conventional methods relying on trial-averaging. As a possible application in this sense, we described the on-line, single-trial reconstruction of arm movement trajectories from multiple single-unit spike trains using dynamic population vectors.

#### Acknowledgements

We gratefully acknowledge the comments by M. Diesmann and D. Heck on an earlier version of the manuscript. This research was supported by the Deutsche Forschungsgemeinschaft (DFG), the German-Israeli Foundation for Scientific Research and Development (GIF) and the Human Frontier Science Program (HFSP).

#### References

- Aertsen A, Bonhoeffer T, Krüger J. Coherent activity in neuronal populations: analysis and interpretation. In: Caniello ER, editor. *Physics of Cognitive Processes*. Singapore: World Scientific Publishing, 1987:1–34.
- Aertsen A, Gerstein G, Habib M, Palm G. Dynamics of neuronal firing correlation: modulation of ‘effective connectivity’. *J Neurophysiol* 1989;61:900–17.
- Arieli A, Sterkin A, Grinvald A, Aertsen A. Dynamics of ongoing activity: explanation of the large variability in evoked cortical responses. *Science* 1996;273:1868–71.
- Azouz R, Gray CM. Cellular mechanisms contributing to response variability of cortical neurons in vivo. *J Neurosci* 1999;19:2209–23.
- Bowman AW. *Applied Smoothing Techniques for Data Analysis: The Kernel Approach with S-Plus Illustrations*, volume 18 of Oxford Statistical Science Series. Oxford: Oxford University Press, 1997.
- Chapin JK, Moxon KA, Markowitz RS, Nicolelis MA. Real-time control of a robot arm using simultaneously recorded neurons in the motor cortex. *Nature Neurosci* 1999;2:664–70.
- Cox DR, Isham V. *Point Processes*. Monographs on Applied Probability and Statistics. London: Chapman and Hall, 1980.
- Diesmann M, Rotter S, Gewaltig MO, Aertsen A. Estimating the temporal accuracy of neural spike responses. In: Schnitzler H, Elsner N, editors. *Brain and Evolution*. Proc 24th Göttingen Neurobiology Conference, volume 2. 1996; 474.
- Georgopoulos AP, Kalaska JF, Caminiti R, Massey JT. On the relations between the direction of two-dimensional arm movements and cell discharge in primate motor cortex. *J Neurosci* 1982;2:1527–37.
- Gerstein GL, Kiang NY-S. An approach to the quantitative analysis of electrophysiological data from single neurons. *Biophys J* 1960;1:15–28.
- Gerstein GL, Aertsen AMHJ. Representation of cooperative firing activity among simultaneously recorded neurons. *J Neurophysiol* 1985;54:1513–28.

- Gielen C, Hesselmann G, Johannesma P. Sensory interpretation of neural activity patterns. *Math Biosci* 1988;92:15–35.
- Grün S, Diesmann M, Grammont F, Riehle A, Aertsen A. Detecting unitary events without discretization of time. *J Neurosci Meth* 1999; this volume.
- Hesselmann G, Johannesma P. Spectro-temporal interpretation of activity patterns of auditory neurons. *Math Biosci* 1989;93:31–51.
- Johannesma P. Neural representation of sensory stimuli and sensory interpretation of neural activity. In: Szekeley G, Labos E, Damjanovich S, editors. *Neural Communication and Control*, volume 30 of *Advances in Physiological Science*. Oxford/Elmsford: Pergamon Press, 1981:103–25.
- Moran DW, Schwartz AB. Motor cortical representation of speed and direction during reaching. *J Neurophysiol* 1999; (in press).
- Nawrot M, Rotter S, Aertsen A. Firing rate estimation from single trial spike trains. In: Elsner N, Waessle H, editors, *Göttingen Neurobiology Report 1997*, Stuttgart: Thieme, volume 2. 1997; 623.
- Nawrot M, Rotter S, Riehle A, Aertsen A. Variability of neuronal activity in relation to behaviour. In: Elsner N, Eysel U, editors, *Proceedings of the 1st Göttingen Neurobiology Conference of the German Neuroscience Society 1999*, Stuttgart: Thieme, volume 1. 1999; 101.
- Nicolelis MAL. *Methods for Neural Ensemble Recordings*. Boca Raton, Florida: CRC Press, 1998.
- Parzen E. On estimation of a probability density function and mode. *Ann of Math Stat* 1962;33:1065–76.
- Paulin MG. Digital filters for firing rate estimation. *Biol Cybern* 1992;66:525–31.
- Richmond BJ, Optican LM, Podell M. Temporal encoding of two-dimensional patterns by single units in primate inferior temporal cortex: I: response characteristics. *J Neurophysiol* 1987;57:132–46.
- Richmond BJ, Optican LM, Spitzer H. Temporal encoding of two-dimensional patterns by single units in primate primary visual cortex: I: stimulus-response relations. *J Neurophysiol* 1990;64:351–69.
- Riehle A, Grün S, Diesmann M, Aertsen A. Spike synchronization and rate modulation differentially involved in motor cortical function. *Science* 1997;278:1950–3.
- Sanderson AC. Adaptive filtering of neuronal spike train data. *IEEE Trans Biomed Eng* 1980;BME–27:271–4.
- Schwartz AB. Direct cortical representation of drawing. *Science* 1994;265:540–2.
- Scott DW. *Multivariate Density Estimation: Theory, Practice, and Visualisation*. Wiley Series in Probability and Mathematical Statistics. Chichester/New York: John Wiley, 1992.
- Silverman B. *Density Estimation for Statistics and Data Analysis*. London: Chapman & Hall, 1986.
- Szücs A. Application of the spike density function in analysis of neuronal firing patterns. *J Neurosci Meth* 1998;81:159–67.